Fractography of Human Hair

Y. K. KAMATH and H.-D. WEIGMANN, *Textile Research Institute, Princeton, New Jersey 08540*

Synopsis

The fracture behavior of human hair has been investigated with a view toward delineating fracture mechanisms that lead to different types of fracture under tensile loading. Principally, three types of fracture are encountered—smooth fractures, step fractures, and fractures involving undefined fibrillated ends. The moisture content of the fiber plays an important role in determining the type of fracture that occurs. Fibers conditioned at either low (~0%) or high (90%) relative humidity give predominantly smooth fractures, whereas those conditioned at intermediate relative humidities give predominantly step fractures. Surface treatments with polymers or surfactants do not seem to have any effect on the strength or the fracture behavior of fibers. At low moisture contents, fracture initiation occurs more often in the cortex, whereas, at high moisture contents, fracture almost always initiates at the surface of the fiber, suggesting that the swelling pressure of the cortex plays a significant role in fracture initiation. Fibers with larger cross-sectional areas tend to split along the axis because of the higher probability of encountering flaws or medullary cells which direct cracks along the fiber axis. Unlike synthetic polymeric fibers, hair fibers seem to follow the Griffith criterion of brittle fracture. This may be coincidental since electron microscopic evidence suggests that fracture propagation occurs by secondary cracks generated as a result of stress concentrations building up at the periphery of the primary crack. The rate of stress transfer to adjacent cortical cells via intercellular cement probably plays an important role in the fracture mechanism.

INTRODUCTION

The fracture behavior of human hair has significant implications for its aesthetic appearance. Grooming, especially of long hair, by combing and brushing can lead to fiber breakage if tangles are encountered during a brushing or combing stroke. Such tangles are most frequently encountered at the tip end of a hair assembly in which the fibers have undergone significant cuticle depletion. Hair breakage occurs either under the influence of excessive bending strains in entanglements or if fibers are subjected to sufficiently high tensile strains. Thus, fracture can occur anywhere along the hair assembly and need not be confined to the tip end of the assembly. Fiber breakage in the tip region frequently leads to split ends because the depleted cuticle no longer protects the fiber from lateral disruption during the post-fracture dissipation of elastic energy.

Earlier work in this area[1–3] has shown that hair fractures can be classified into three principal patterns depending on the nature of the resulting fiber ends. These fracture patterns are: (1) smooth fractures, where the fracture occurs in a single plane perpendicular to the fiber axis; (2) step fractures, where fracture initiates in a plane (or planes) perpendicular to the fiber axis and results in splitting of the fiber along the axis (there could be multiple steps in such a process); and (3) fibrillation, where the fracture end is split open and has the appearance of the bristles of a paint brush.

Recently, a number of hair care formulations containing polymeric substances

Journal of Applied Polymer Science, Vol. 27, 3809–3833 (1982)
 CCC 0021-8995/82/103809-25$03.50

have been developed which are claimed to have the ability to repair damaged hair fibers. It became of interest to examine the possibility that these topical treatments might affect the fracture behavior of hair fibers. Since most fiber fractures initiate at flaws near the surface of fibers, it is not unreasonable to expect that deposition of polymers might have some effect on the fracture initiation process. This investigation of the fracture of hair fibers under relatively fast tensile loading conditions examines the effect of environmental relative humidity and of surface treatments on the nature of the fracture.

EXPERIMENTAL

Two samples of hair were used in this work. One of them was obtained from a 26-year-old female of European origin (Sample J). The other was a commercial sample obtained from DeMeo Brothers of New York. This hair is specified as European dark brown hair (EDBH) and is presumed not to be from a single individual. The hair samples were cleaned by sequential extraction with chloroform/methanol/chloroform, followed by exhaustive rinsing in distilled water.

Tensile fracture measurements were carried out on specimens 50.8 mm long using an Instron tensile tester equipped with an environmental chamber. The specimens, mounted on tabs, were conditioned for 2 days prior to the measurements over solutions giving appropriate humidities. Unless indicated otherwise, the strain rate in these measurements was 0.033/s (200%/min).

The polymers JR-400 (Union Carbide) and Gafquat-755 (GAF-755, GAF Corp.) and the low molecular weight surfactant Triton-X-400 (TR-X-400, Rohm & Haas) were used in this study. Fiber treatments were carried out at room temperature (~25°C) with a 1% solution of the polymer or surfactant for 0.9 and 3.6 ks, followed by two rinses with distilled water and conditioning at the selected humidity.

Fracture ends were examined on a JEOL-JSM-12 scanning electron microscope after sputtering with gold. Axial splitting lengths were determined on an optical microscope.

RESULTS AND DISCUSSION

Effect of Humidity on Tensile Mechanical Properties and Axial Splitting Behavior

Mechanical properties: The distributions of initial modulus, breaking stress, and breaking extension are shown in the form of box plots[4] in Figures 1(a), 1(b), and 1(c), respectively. The characteristic features of a typical box plot are included in Figure 1(a). The size of a notch is determined using $C = 1.76$ ($1.25\ R/1.35\ \sqrt{N}$), where R is the interquartile range and N is the number of specimens. The difference between the medians of interest is said to be statistically significant (in this case at the 95% confidence level) if the notches about the medians do not overlap.

Of the three mechanical properties, initial modulus is known to be the most sensitive to moisture due to hydrogen bond breakage, and this is seen clearly in Figure 1(a). Sample J seems to be more sensitive than EDBH. The initial moduli of EDBH fibers do not change significantly as the relative humidity is

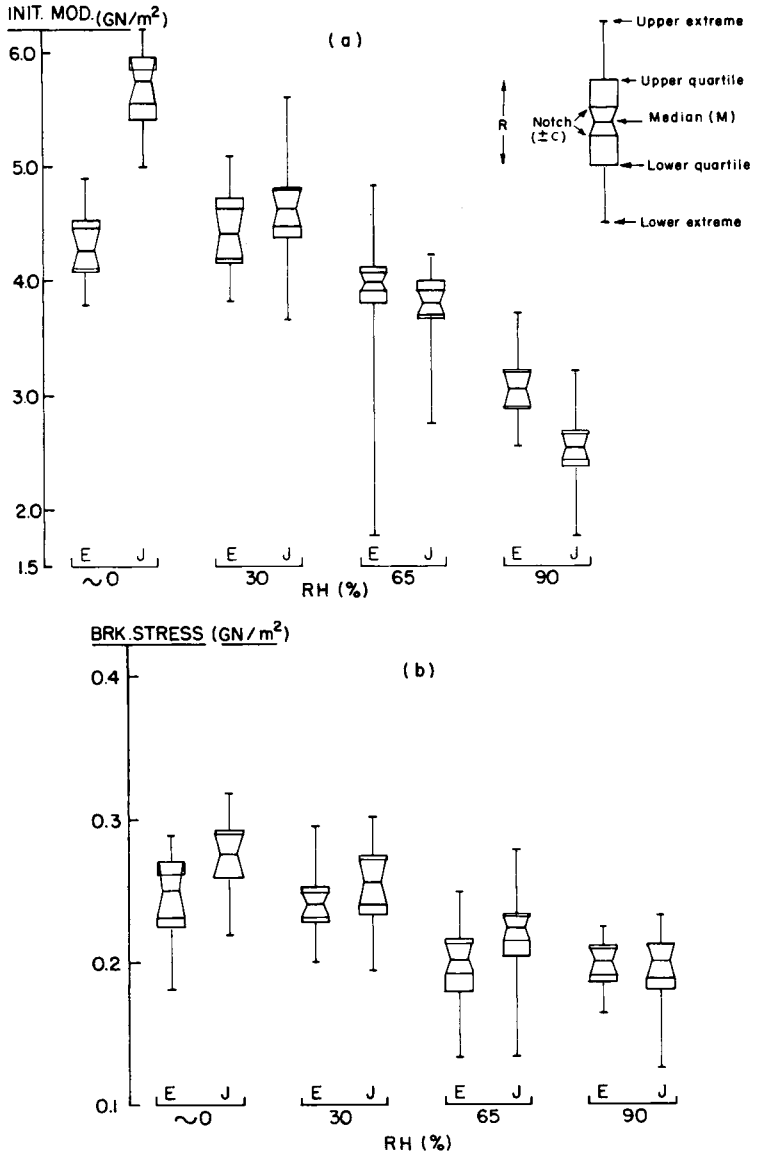

Fig. 1. Box plots of the mechanical properties of hair samples EDBH (E) and J as a function of relative humidity: (a) Initial modulus; features of a typical box plot at upper right; (b) breaking stress; (c) break elongation.

increased from 0% to 30%. It should be noted that measurements at 0% RH were carried out as quickly as possible in the environmental chamber containing Drierite® and P_2O_5, after drying the fibers over P_2O_5 for a week. A significant decrease is observed when RH is increased to 65% and higher values. Initial moduli of sample J fibers are higher than those of EDBH at 0% RH, whereas they are significantly lower at 65% and higher RH. At 30% RH the difference between the two samples is not significant.

With both samples the breaking stress is less sensitive to moisture than the initial modulus. The breaking stress for EDBH and sample J is significantly

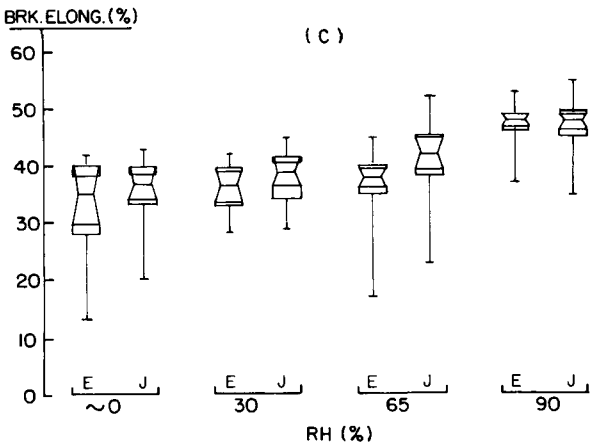

Fig. 1. (*Continued from previous page.*)

lower at 65% and 90% RH than at 0% and 30% RH, but the differences are not significant within these two ranges of relative humidity. On the other hand, for sample J the breaking stress is significantly higher at 65% RH than at 90% RH. The difference between the breaking stresses of EDBH and sample J are not significant at any other relative humidity than 65% RH.

Breaking elongation is probably the property least sensitive to moisture. For both samples the breaking elongation is not significantly different up to 65% RH, but is significantly higher at 90% RH than at lower humidities. Comparing box plots for samples EDBH and J, it is seen that only at 65% RH is there a barely significant difference between them.

Fracture behavior: Most of the fractures obtained under various relative humidity conditions were either smooth [Fig. 2(a)] or step fractures [Fig. 2(b)]. A few of the fibers had fibrillated or poorly defined fractured ends; these will be discussed elsewhere.

The length of axial splitting [distance AB in Fig. 2(b)] was measured with an optical microscope, and distributions of axial splitting lengths at various relative humidities are shown in Figures 3 and 4 for EDBH and sample J, respectively. It should be noted that these distributions are based on smooth (crosshatched areas on the first bar) and step fractures only. Because of the relatively small sample size, most of the distributions in this work are not well defined. Therefore, it is difficult to draw conclusions regarding the effect of specific experimental conditions on the fracture behavior at a high level of confidence (~95%) by comparing the various distributions.

An alternative approach is to divide the population of fracture ends into two groups, i.e., smooth (axial splitting length = 0) and step (axial splitting length > 0) fractures as shown in Table I for EDBH and sample J. From these data χ^2 values can be calculated[5] by choosing two pairs of values at relative humidities for which comparison is to be made. For example, to establish whether the axial splitting pattern at 30% RH is different from that at 0% RH in the case of EDBH, the values from Table I used to calculate χ^2 are: (12;7) and (5;13). Values of χ^2 for 17 such comparisons are given in Table II.

The probability of obtaining one significant comparison by chance is given by $1 - (1 - \alpha)^c$, where c is the number of comparisons made (in this case 17).[6]

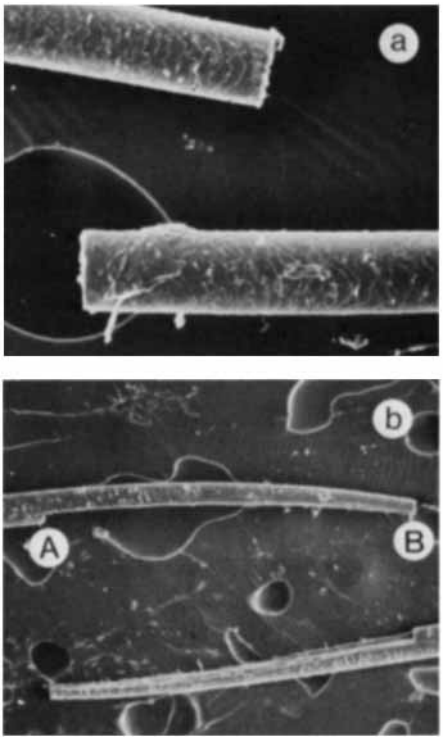

Fig. 2. Smooth (a, 400 ×) and step (b, 140 ×) fractures of EDBH.

A value of α at the 95% confidence level can be obtained from the equation $1 - (1 - \alpha)^{17} = 0.05$. A value of 0.003 is obtained for α. The value of χ^2 at this value of α for one degree of freedom (because the number of variables is 2, i.e., smooth or step fracture) is 9.354. Based on this criterion, only 6 out of 17 comparisons are significant at the 95% confidence level (underlined in Table II), and several conclusions are drawn from these results:

(1) In fibers of both samples significantly fewer step fractures are observed at 90% RH than at 30% and 65% RH.

(2) In fibers of sample J a significant increase in the number of step fractures is observed at 65% RH over the number at 0% RH. This is not observed in the case of EDBH and hence is a distinguishing feature of sample J, especially, in view of the split end problem the sample is known to have.

TABLE I
Effect of Relative Humidity on the Fracture Pattern Distribution of EDBH and Sample J

RH (%)	EDBH			J		
	Total no. specimens	Smooth	Step	Total no. specimens	Smooth	Step
~0	19	12	7	19	12	7
30	18	5	13	29	8	21
65	127	71	56	89	17	72
90	23	21	2	35	25	10
Wet	—	—	—	32	22	10

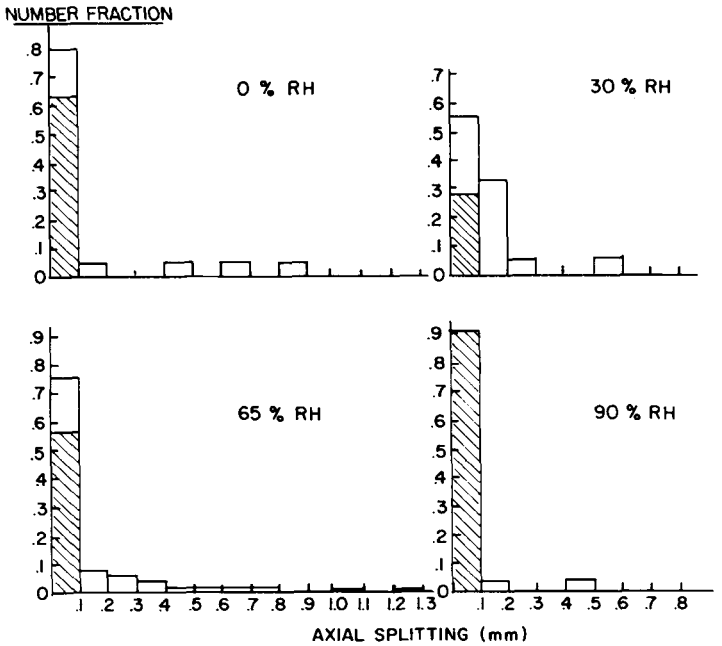

Fig. 3. Distributions of axial splitting lengths for EDBH at various relative humidities. Cross-hatched areas represent smooth fractures.

(3) Fracture patterns of EDBH and J are significantly different at 65% RH. At this relative humidity sample J gives a larger number of step fractures, in agreement with the observations made above.

Effect of Rate of Extension

For this study measurements were performed at 65% RH on specimens taken from the root end of the fibers. The distributions of axial splitting length based on ~20 fibers (excluding those with undefined fracture ends) are shown in Figures

TABLE II

χ^2 Values[a] for Comparison of Fracture Pattern Distributions at Various Humidities

Sample ↓→	RH (%) ↓→	EDBH ~0	EDBH 30	EDBH 65	EDBH 90	J ~0	J 30	J 65	J 90	J Wet
EDBH	~0					0				
	30	4.6587					0.0002			
	65	0.3543	5.0009					29.36		
	90	4.8958	17.564	10.289					3.3414	
J	~0									
	30					5.976				
	65					15.473	0.9431			
	90					0.3905	12.206	30.710		0.0573
	Wet									

[a] $\chi^2_{0.003,1}$ = ~9.354 (interpolated).

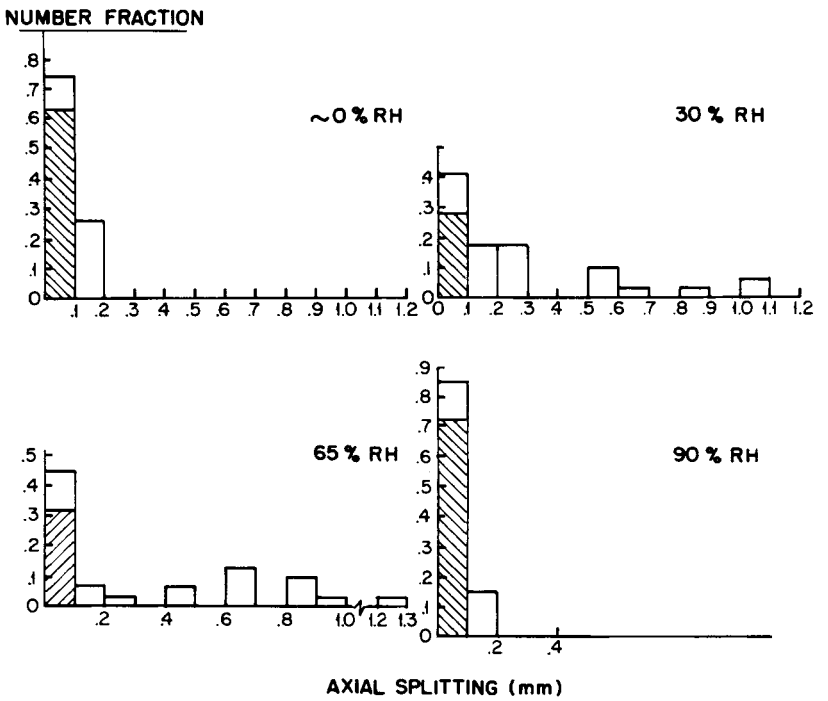

Fig. 4. Axial splitting lengths in the tensile fracture of fibers from sample J at various relative humidities. Crosshatched areas represent smooth fractures.

5 and 6 for samples EDBH and J, respectively. The differences between them with regard to smooth and step fractures are not significant at the 95% confidence level according to the χ^2 test described earlier. However, there seems to be a general trend towards more smooth fractures with increasing rate of extension, suggesting that high rates of extension prevent the diversion of the crack in the axial direction. This may be associated with stress transfer, which is faster to elements ahead of the crack than normal to the initial crack direction. Such stress transfer prevents high stress concentrations at the crack tip which are known to be responsible for crack diversion.[7] As will be discussed later, the intercellular cement between cortical cells may play a part in the stress transfer mechanism.

Effect of Weathering and Mechanical Damage

These effects are generally studied by comparing measurements on root and tip ends of fibers, since, especially for long hair, tip ends have been exposed to much more severe environmental and mechanical stresses than the corresponding root ends. Measurements were made at 65% RH (since the highest degree of axial splitting was observed at this RH) on the root and tip ends of the same fibers from samples EDBH and J, and the distributions of axial splitting lengths are shown in Figures 7 and 8, respectively.

In the case of EDBH, root ends give a larger number of smooth fractures than tip ends. This is in agreement with earlier work indicating that an undamaged cuticle structure prevents step fractures by preventing splitting along the fiber axis,[2] and reflects the fact that the tip ends of these fibers have lost a significant amount of cuticle by weathering and mechanical damage.

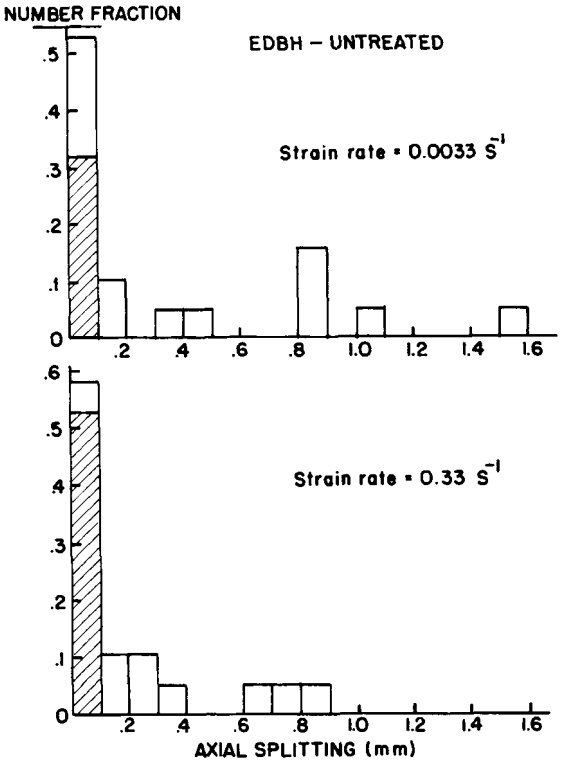

Fig. 5. Effect of strain rate on the axial splitting of EDBH.

For specimens of sample J the difference between the root and tip ends is not significant, but, surprisingly, root ends give relatively fewer smooth fractures than the tip ends. The generalization that smooth fractures are favored when the cuticle is undamaged may not be applicable to sample J which, as was pointed

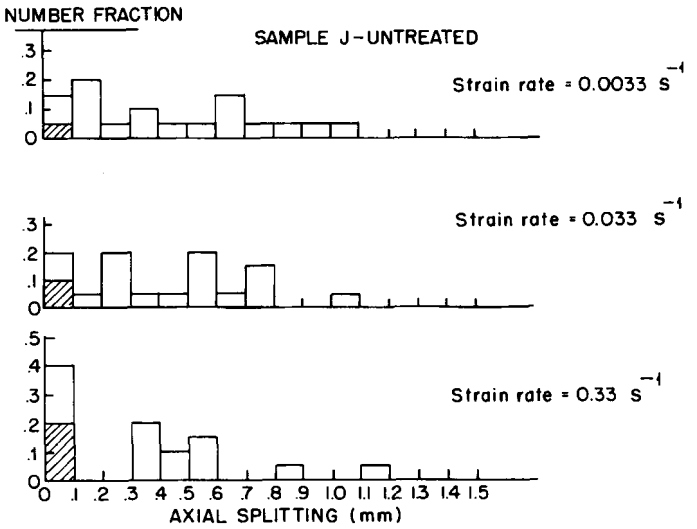

Fig. 6. Effect of strain rate on the axial splitting of sample J.

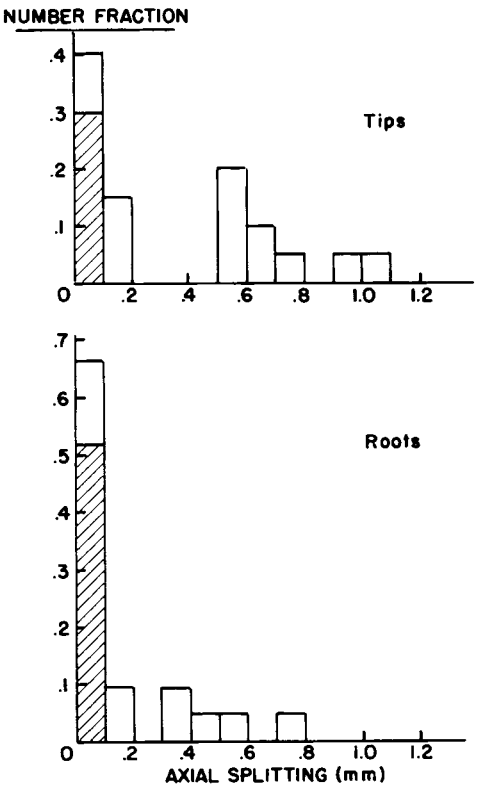

Fig. 7. Axial splitting length distributions of tips and roots of EDBH at 65% RH.

out above, is known to be prone to split ends. Measurements on larger samples are necessary to establish whether this pattern holds.

The role of the cuticle in axial splitting was studied by abrading fiber specimens of sample J consecutively with emery paper of grades 280, 320, and 400. Some of the specimens were examined microscopically to check the extent of cuticle removal. Fibers were also vibroscoped before and after abrasion, to establish changes in diameters, assuming that the modulus remains unchanged. An average reduction in diameter of ~7.7 μm was observed, suggesting that most of the cuticle may have been removed. Distribution of axial splitting lengths shown in Figure 9 indicate that abraded fibers show a tendency towards longer axial splitting lengths. This observation suggests that a strong intact cuticle does indeed decrease the extent of splitting in the axial direction. In some abraded specimens axial splitting proceeded further than the length of the step (Fig. 10), an occurrence not commonly seen in step fractures.

Effect of Surface Treatments

The distribution of smooth and step fractures in a relatively small sample of fibers from EDBH and sample J treated with the two polymers and the surfactant for 0.9 and 3.6 ks is shown in Figures 11 and 12, respectively. All these measurements were performed at 65% RH. Statistical analysis of fracture pattern distributions and mechanical properties by the methods described earlier showed

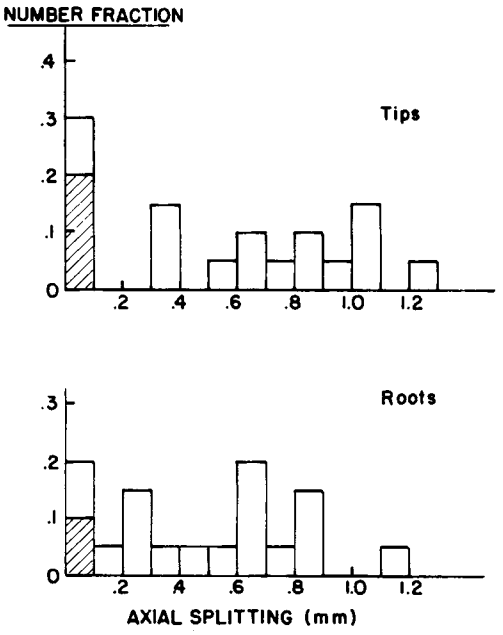

Fig. 8. Axial splitting length distribution of tips and roots of fibers of sample J at 65% RH.

no significant effect of the surface treatments. This suggests that polymers applied to the hair surface do not "repair" the flaws which are known to be responsible for fracture. However, this conclusion does not mean that the polymers do not protect the fiber surfaces from mechanical wear and damage that result from grooming procedures. In fact, such protection may be one of the most important functions of surface-deposited polymers.

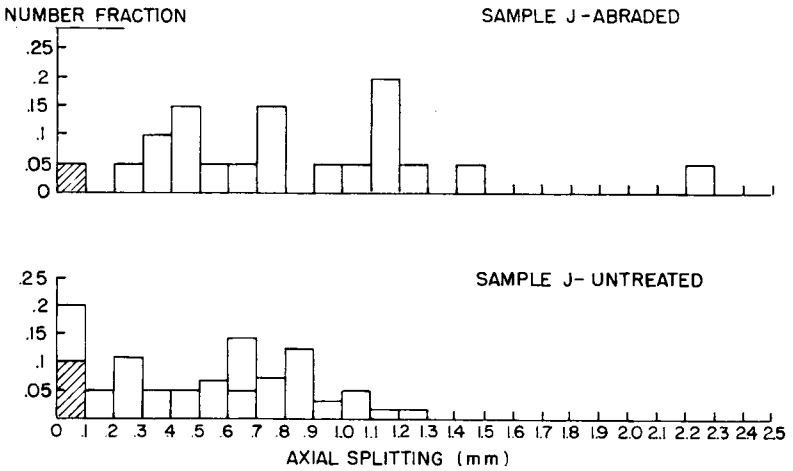

Fig. 9. Axial splitting length distributions in abraded fibers of sample J at 65% RH.

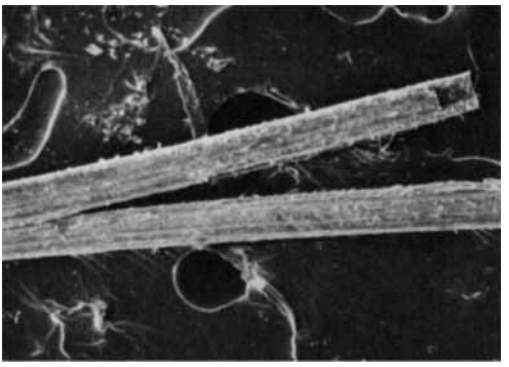

Fig. 10. Axial splitting in abraded hair fiber from sample J (150 ×).

Fracture Mechanisms

Smooth fractures: In an effort to understand the mechanisms underlying the formation of smooth and step fractures, the ends of the fractured fibers were examined in a scanning electron microscope. As noted above, smooth fractures occurred under all conditions, but their number relative to other kinds of fractures varied according to the relative humidity of the environment. Scanning electron micrographs (SEM's) of smooth fracture ends of EDBH specimens broken at 65% RH are shown in Figures 13 and 14. These micrographs clearly show that the fractures initiated at surface flaws and radiated across the fibers in a plane perpendicular to the axis, giving rise to a "cut with a razor" type of appearance. Smooth fractures of sample J also show this kind of behavior, although the nature of the flaw at which crack initiation occurs may be different.

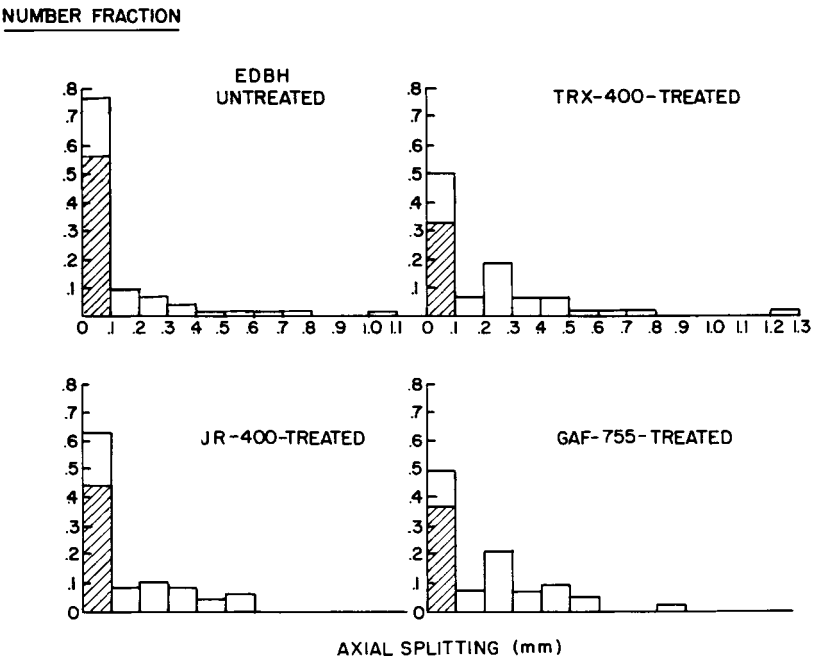

Fig. 11. Axial splitting length distributions in treated EDBH at 65% RH.

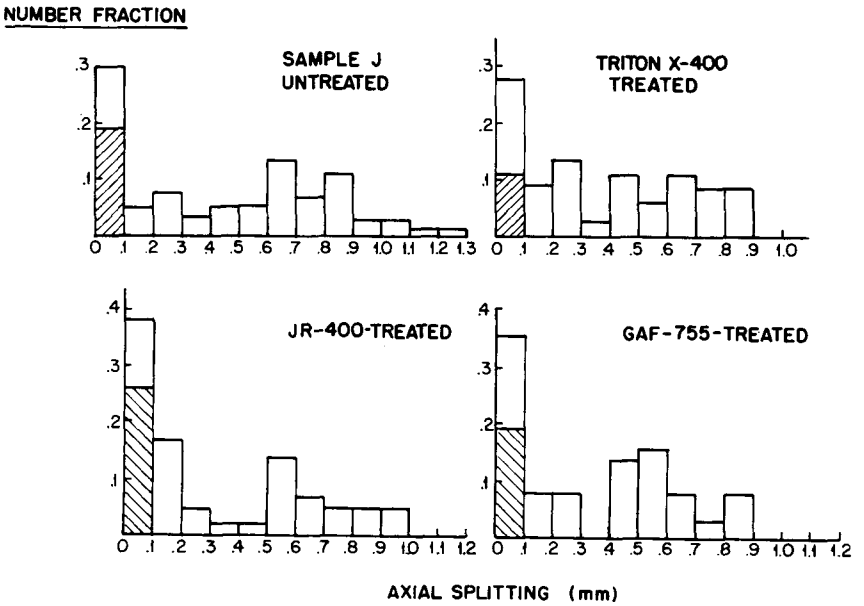

Fig. 12. Axial splitting length distributions in treated sample J fibers at 65% RH.

For example, in Figure 13(a) the flaw seems to be an inherent defect in the fiber. In Figure 14(a) the crack seems to have initiated near the periphery of the fiber where an inherent defect is seen. The fracture face can generally be divided into smooth and coarse sections as will be discussed in detail shortly. A closer examination of Figures 14(a) and 14(b) shows that the fracture does not occur exactly in a plane (as in glass, for example) but is confined to a narrow region in such a way that the depressions in one fracture face match with the protuberances in the other.

At higher humidity and in the wet condition there are more smooth fractures than any other type. The nature of the fracture faces is basically the same as at 65% RH, exhibiting a smooth and a coarse region, except in some cases (especially in the wet condition) where no crack initiation can be detected and the entire fracture face has a coarse appearance. This is shown in Figure 15(b)

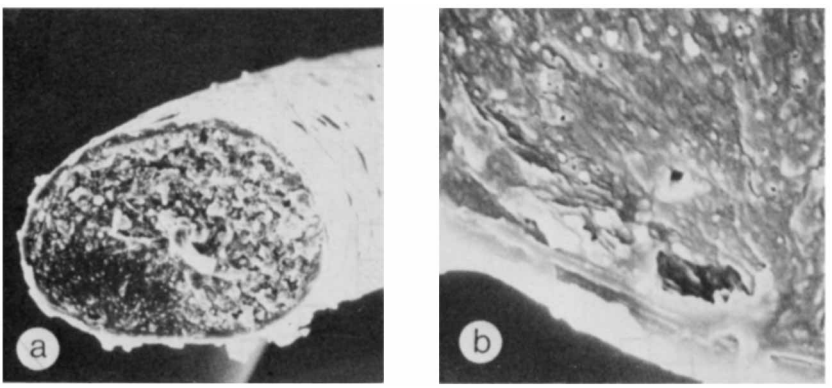

Fig. 13. Smooth fracture end of an EDBH fiber at 65% RH: (a) Fracture face (1000 ×); (b) magnified flaw (6000 ×). Cuticle layers near the flaw can be seen.

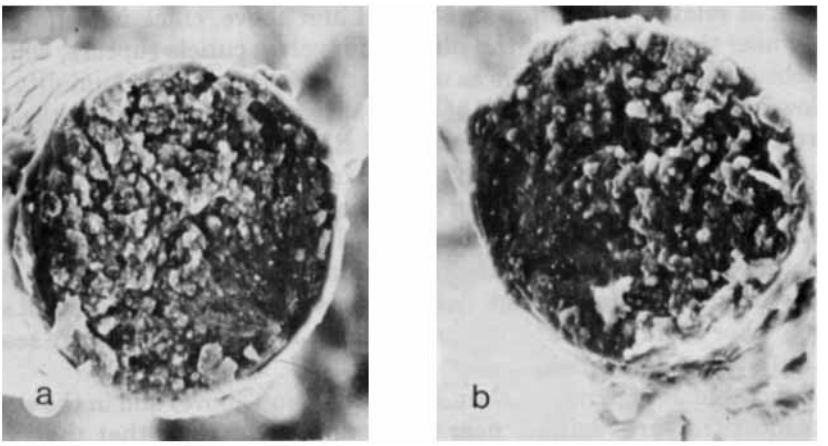

Fig. 14. Matching fracture faces of an EDBH fiber at 65% RH. Both at 1000 ×. Note smooth and coarse areas.

for a wet fiber of sample J. Smooth fractures with smooth and coarse regions are also seen in wet fibers [Fig. 15(c)], although the demarcation between the two regions is not well defined. Fibers conditioned to 90% RH show similar smooth fractures [Fig. 15(a)], but secondary cracks are initiated near the periphery of the slow segment [see arrows in Fig. 15(a)].

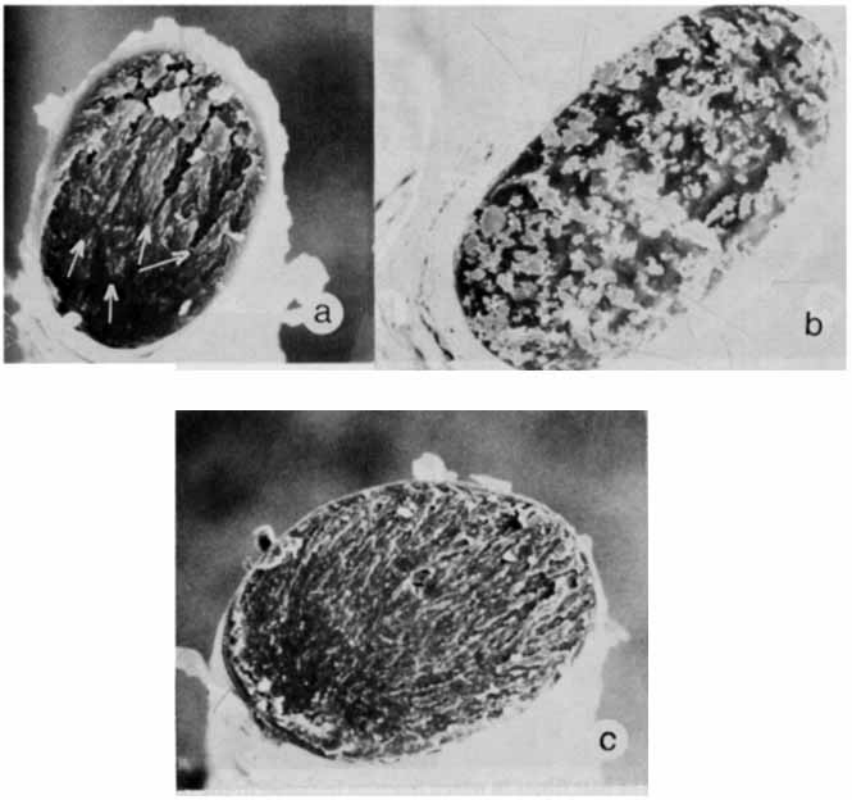

Fig. 15. Smooth fractures of sample J fibers: (a) 90% RH; (b, c) wet fibers.

Thus, at relative humidities of 65% RH and above, crack initiation occurs mostly near the periphery of the fiber and involves cuticle rupture, which has been observed by other authors as well.[2,8] When the relative humidity is 30% and lower, an increasing number of fibers shows crack initiation in the cortex. Figure 16(c) shows an EDBH fiber at 30% RH with a crack initiated near the center. This may not be a perfectly smooth fracture, for the coarse region seems to be in a slightly higher plane than the smooth region. EDBH fibers dried for a week over P_2O_5 clearly show crack initiation in the cortex [Figs. 16(a) and 16(b)]. The nature of the flaws at which the crack initiation occurs is not clear. However, in some cases, the medullary region of the fibers seems to be an important source of flaws. For example, in a dry fiber of sample J [Fig. 16(d)] fracture seems to have initiated on the periphery of the medulla.

The fact that at high relative humidities (65% and above) and in the wet condition most fractures initiate near the periphery suggests that the swelling pressure of the cortex on the cuticle contributes to the crack initiation process. Forces that contribute to fracture initiation are shown schematically in Figure 17. It is suggested that, in addition to the tensile force acting in opposite directions along the fiber axis, the swelling pressure of the cortex and Poisson contraction lead to cuticle rupture and crack initiation at the interface between cuticle and cortex. The crack then propagates towards the center of the cortex. As the relative humidity is lowered, the swelling pressure of the cortex on the cuticle decreases. In the extreme case of fibers dried over P_2O_5 (~0% RH), rel-

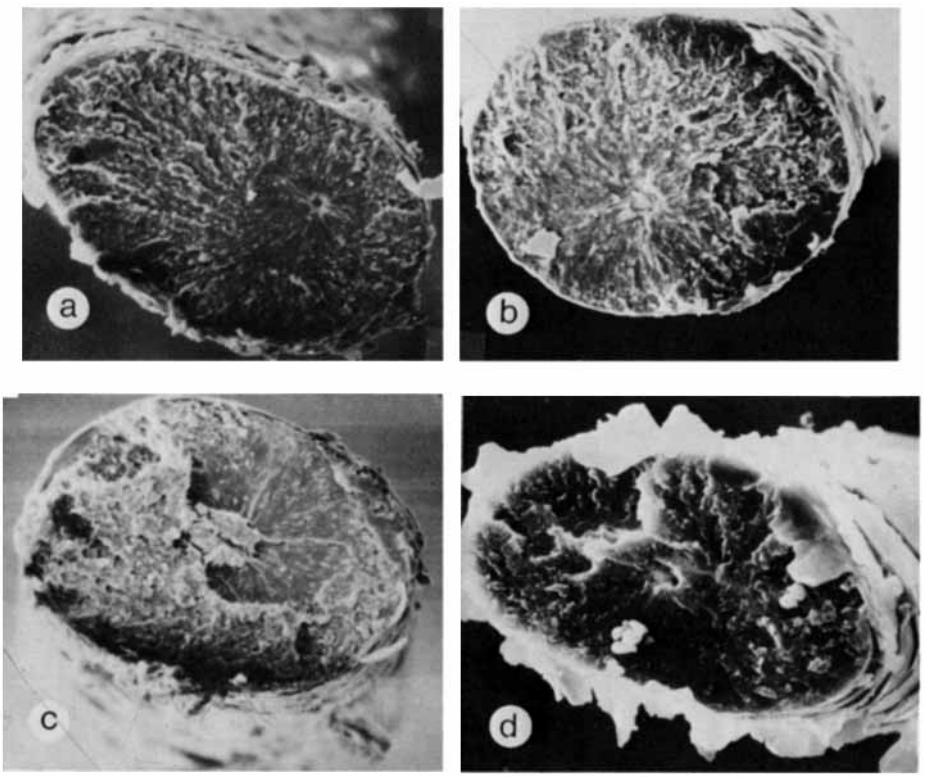

Fig. 16. Smooth fractures of hair fibers in which fracture initiated in the cortex (1000 ×): (a, b) EDBH at ~0% RH; (c) EDBH at 30% RH; (d) sample J at ~0% RH.

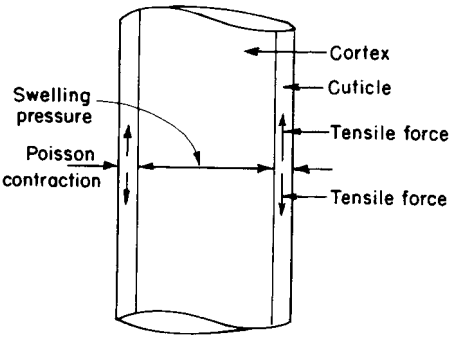

Fig. 17. Schematic representation of the forces acting on the cuticle of a swollen fiber subjected to tensile loading.

ative movement of cuticle cells requires less force than deformation of the cortex when the fiber is subjected to tensile loading. This would lead to stress concentrations and fracture initiation within the cortex itself.

Fracture of Synthetic Fibers and Its Relationship to Hair Fracture: Since fracture patterns encountered in hair fibers are similar to those observed in acrylic[9] and nylon[10] fibers, the fracture mechanisms may be similar. As in the case of hair, fracture faces of synthetic fibers show a smooth region generated by slow propagation of the crack. A coarser region is generated by the much faster propagation of the crack during catastrophic failure of the fiber. The smooth and coarse regions are referred to as "slow" and "fast," referring to the processes that give rise to these appearances. It is known that synthetic fibers do not follow Griffith's criterion of fracture (which is strictly applicable to brittle materials) because of their elasticity. Lamb[10] has shown this in the case of nylon 6. Following his procedure, breaking load can be calculated for hair fibers from

$$F_B = \sigma^* \cdot A_F$$

where A_F is the area of the fast segment in the fracture face and σ^* is the critical stress according to Griffith's equation

$$\sigma^* = [E\rho/c]^{1/2}$$

where E is the modulus, ρ is the surface energy ($\sim$1.0 kJ/m^2), and c is the critical size of the crack (depth of the slow segment). According to this analysis, conformity with the Griffith criterion is indicated by the independence of the breaking load of the area of the fast segment.

Following the above procedure, breaking loads were calculated for hair fibers which had given smooth fractures at various relative humidities. Since these fibers break in the postyield region, the postyield modulus was used in the Griffith equation. The breaking loads for fibers from EDBH and sample J as a function of relative area of the fast segment are shown in Figures 18 and 19, respectively. Two groups of fibers were selected based on their cross-sectional areas, A_1 and A_2, as measured using the vibroscope: $A_1 \approx 3.4 \times 10^{-9}$ m^2 and $A_2 \approx 5.2 \times 10^{-9}$ m^2. From these plots it can be seen that EDBH and sample J show similar behavior, as do the two groups of fibers of different cross-sectional area. Most of these fibers have A_F/A values of 0.6–0.8, except for EDBH at $\sim$0% RH

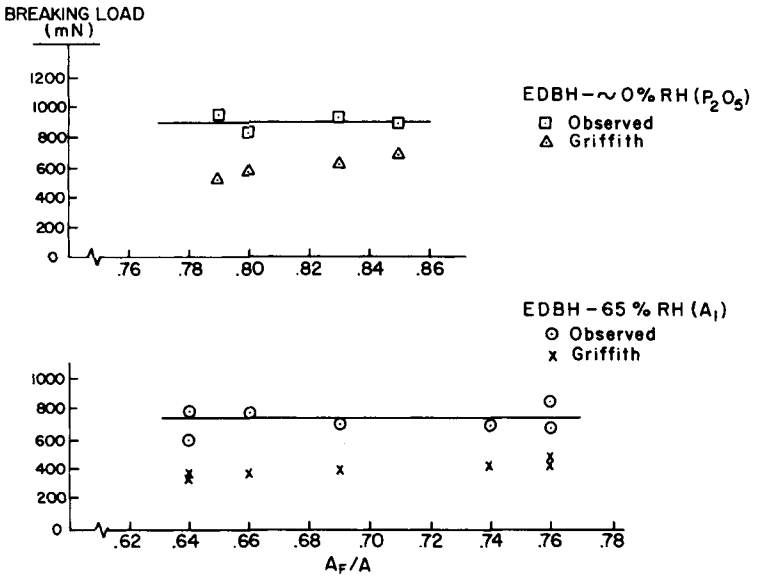

Fig. 18. Relationship of measured and calculated breaking loads to the relative area of the fast segment. EDBH at ~0% RH (P_2O_5) and 65% RH (A_1): (⊡, ⊙) observed; (△, ×) Griffith.

with values ranging from 0.78 to 0.86. It should be noted that the Griffith criterion is applicable only when the relative crack size is small ($A_F/A > 0.8$). Although the observed loads are somewhat higher than those calculated using the Griffith equation, both are virtually independent of the area of the fast segment. This would suggest that the Griffith criterion is applicable to the fracture behavior of hair.

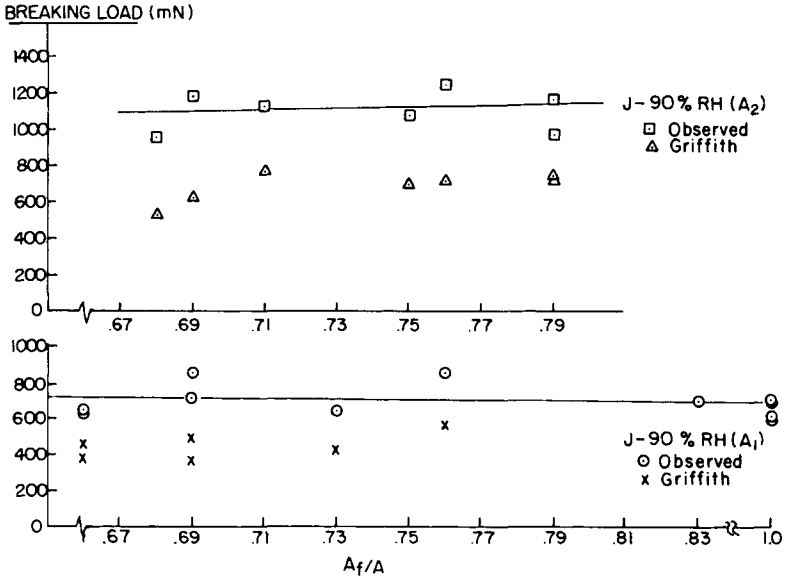

Fig. 19. Relationship of measured and calculated breaking loads to the relative area of the fast segment. Sample J, 90% RH: (⊡, ⊙) observed; (△, ×) Griffith.

TABLE III
Specific Surface Energy of Fracture of EDBH Fibers at ~0% RH

r^* (μm)	ρ (kJ/m^2)
13.3	1.68
14.3	1.67
12.0	1.68
14.5	1.68

To check this further, the specific fracture surface energy ρ was calculated for four EDBH fibers that gave circular cracks in the cortex with critical radius r^*, using the equation

$$r^* = \rho E/2(1 - \mu^2)\sigma^2$$

where μ is Poisson's ratio (assumed to be 0.5) and σ is the breaking stress. It should be noted that the radius of the circular crack visible in the SEM's [Figs. 16(a) and 16(b)] is assumed to be the critical radius. The postyield modulus was again used in these calculations. As shown in Table III, the measured crack size from SEM's is quite constant from fiber to fiber, and reasonable values are obtained for the specific fracture surface energy. This gives further support to the applicability of the Griffith criterion to hair under these conditions. However, it is difficult to reconcile the deformation behavior of human hair with the Griffith criterion of brittle fracture.

The apparent applicability of Griffith's criterion to hair fracture and the existence of a critical stress at the end of the slow period of crack propagation strongly suggest that catastrophic failure may be occurring via propagation of secondary cracks initiating near the periphery of the primary crack as a result of stress concentrations. Kies et al.[11] have observed this kind of behavior in poly(methyl methacrylate). The fast segments of the fracture faces of hair fibers show these secondary cracks propagating towards the surface [e.g., Fig. 15(a)]. These secondary cracks may or may not be in line with the original direction of propagation. For example, in Figure 16(a), the direction of propagation of these secondary cracks is different from the radial direction of the primary crack propagation, at least in some parts of the fracture face. This suggests that secondary crack initiation occurs independently as a result of stress concentrations at the periphery of the primary crack. Fracture in the fast segment seems to involve the breaking of rows of cortical cells via rapid stress transfer. The intercellular cement and the presence of medullary cells would be expected to play an important role in this stress transfer mechanism.

A study of the tensile rupture of blended yarn by Monego and Backer[12] seems to have some relevance to the fracture behavior of hair. The authors observed that in a blended yarn (90 filaments, 40/50 cotton/polyester, twist multiple 2.17) multiple breaks of cotton fibers occurred over an extended length of the yarn within the gauge length at various extensions. In a similar structure of twist multiple 3.26 the initial fracture of cotton fibers near the center spread quickly to all cotton fibers in the yarn in a very narrow region leading to catastrophic failure. This observation reflects the effect of fiber cohesion (affected by varying twist) on stress transfer to adjacent filaments. At high fiber cohesion the fracture of filaments near the center leads to catastrophic failure of the entire yarn in a narrowly defined region.

Hair fibers are bundles of cortical cells held in a cuticular sheath, somewhat analogous to a yarn with the intercellular cement controlling cohesion between cells. Cohesion is expected to be good at very low humidity and at very high humidity because of the shrinking and swelling of the cortex, respectively. This promotes rapid stress transfer, leading to a larger number of smooth fractures. At intermediate humidities, a reduction in intercellular cohesion can result in inefficient stress transfer to elements adjacent to the propagating crack, resulting in a larger number of fibers undergoing axial splitting, as is observed with both samples.

The cause of fractures of the kind shown in Figure 15(b), also observed in certain types of acrylic fibers,[9] is not clear. The absence of a primary crack suggests that this type of fracture may belong to the high-speed (explosive) type in which multiple initiations give rise to the appearance of a uniform fracture pattern with no propagating lines. Many elements of the fiber structure reach initial stress at the same time. The other possibility is the generation of a circumferential crack by fast propagation under the action of the load. The cuticle must be under considerable pressure for this to occur. This may be the reason why this kind of fracture, though rare, occurs only at high humidities (90% RH) and in wet fibers.

Step fractures: The structure of a hair fiber resembles that of a composite. In the interior of the cortex, medullary cells can occasionally be found, which are more or less empty structures having cell walls. Sometimes these cells form in a row, giving rise to a continuous channel in the middle of the cortex. Occasionally, medullary cells act like flaws in the fiber at which fracture can initiate. On the other hand, they can also prevent the propagation of a crack. This leads to stress concentrations which are often relieved by diverting the fracture along the axis of the fiber. Basically, there are two mechanisms by which step fractures appear to occur in hair fibers. These are presented schematically and explained in Figures 20(a) and 20(b).

In Figure 21 are shown the fracture ends and faces of a fiber with a step fracture. The medulla running along the fiber axis can be seen on the fracture ends [Fig. 21(a)]. The crack apparently initiated at the periphery of the medulla and propagated towards the surface of the fiber [Fig. 21(b)]. Stress concentrations

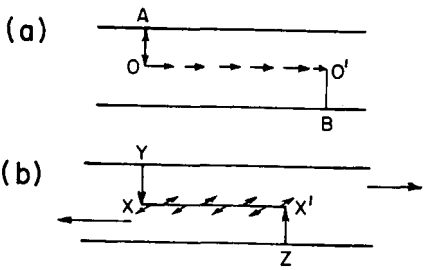

Fig. 20. Representations of two mechanisms for the formation of step fractures. (a) Step 1: Crack initiates at O or A and propagates in the opposite direction; step OA forms the slow segment; Step 2: If crack cannot propagate through the rest of the cross section, stress concentration builds up at O and is relieved by axial splitting to O′; Step 3: Stress builds up on the rest of the cross section and catastrophic fracture occurs at the weakest point O′B (fast segment). (b) Step 1: Cracks simultaneously initiate and propagate along XY and X′Z reaching the interface XX′. Step 2: Tensile load acts like a couple and shears the fiber at the interface XX′.

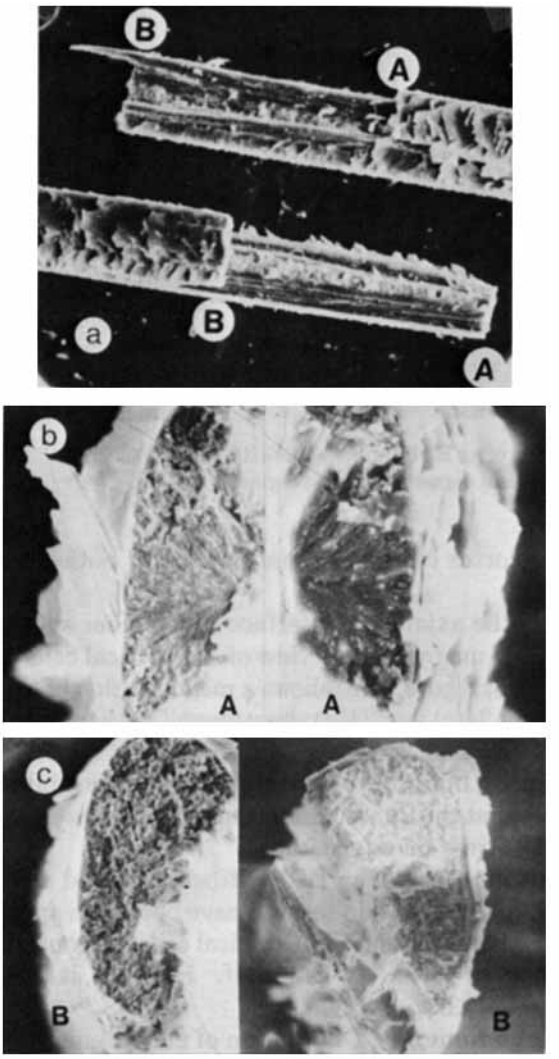

Fig. 21. Fracture ends and faces of a fiber from sample J broken at 30% RH: (a) fracture ends (500 ×); (b) slow step (2000 ×); (c) fast step (1250 ×).

developing at the edge of the propagating crack probably led to axial splitting and catastrophic fracture at step B [Fig. 21(c)]. This clearly indicates that the leading edge of a propagating crack is not necessary for the initiation of catastrophic failure. The appearance of the fast segment suggests that the cortical cells break in the form of a bundle of fibers.

A step fracture of an EDBH fiber in which fracture initiated on the surface is shown in Figure 22. One fracture face [Fig. 22(a)] shows a combination of slow and fast segments; the other consists entirely of a fast segment. The step fractures of Figures 21 and 22 follow the first mechanism diagrammed in Figure 20(a).

The step fracture of an EDBH fiber at low RH shown in Figure 23 seems to have resulted from simultaneous propagation of two cracks perpendicular to the fiber axis separated along the length of the fiber as in Figure 20(b). The initiation

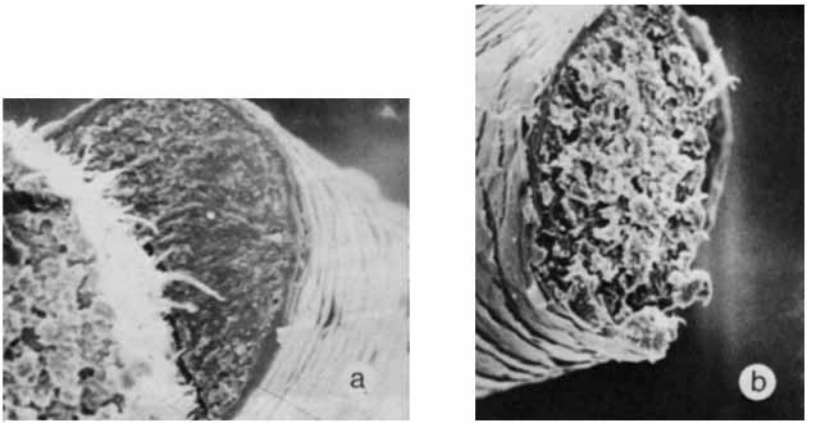

Fig. 22. Step fracture of an EDBH fiber at 65% RH (1250 ×). Crack initiation occurred at the fiber surface: (a) slow–fast segments; (b) fast segment.

of the crack in the cortex can be seen on the faces of both steps as indicated by the arrows.

Figure 24 shows the axial split interface of the fiber shown in Figure 23 in greater detail: a low magnification view of the cortical cells at the interface is shown in Figure 24(a); Figure 24(b) shows a magnification of the region indicated on 24(a); and Figures 24(c) and 24(d) show magnifications of the regions marked on 24(b). These SEM's show that in axial splitting at low RH, cortical cells are usually not torn apart, but failure appears to occur in the intercellular cement. This would suggest that the intercellular cement is weaker than the cortical cells and hence acts as a stress release medium.

In the axial split interface of an EDBH fiber fractured at 65% RH (Fig. 25), on the other hand, cortical cells do seem to have been torn apart. It would seem that under these higher RH conditions cortical cells are considerably weakened, so that failure can occur within the cell itself. However, it should be noted that this does not occur very frequently.

Postfracture phenomena: Dissipation of elastic energy from the point of fracture appears to play an important role in the nature of fracture ends.[13]

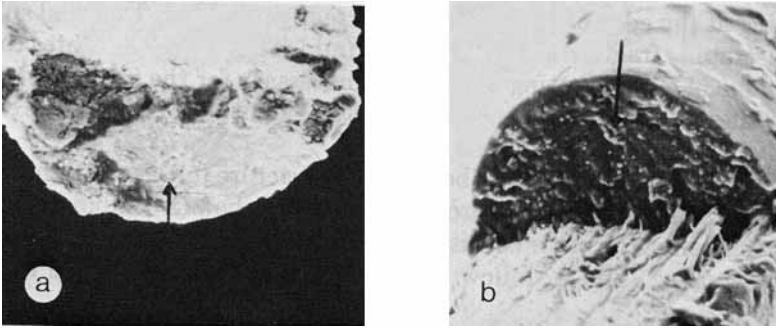

Fig. 23. Step fracture of an EDBH fiber dried over P_2O_5 and fractured at ~0% RH. These are not matching fracture faces but the two steps of one of the fiber ends. Arrows indicate crack initiation: (a) 3000 ×; (b) 1300 ×.

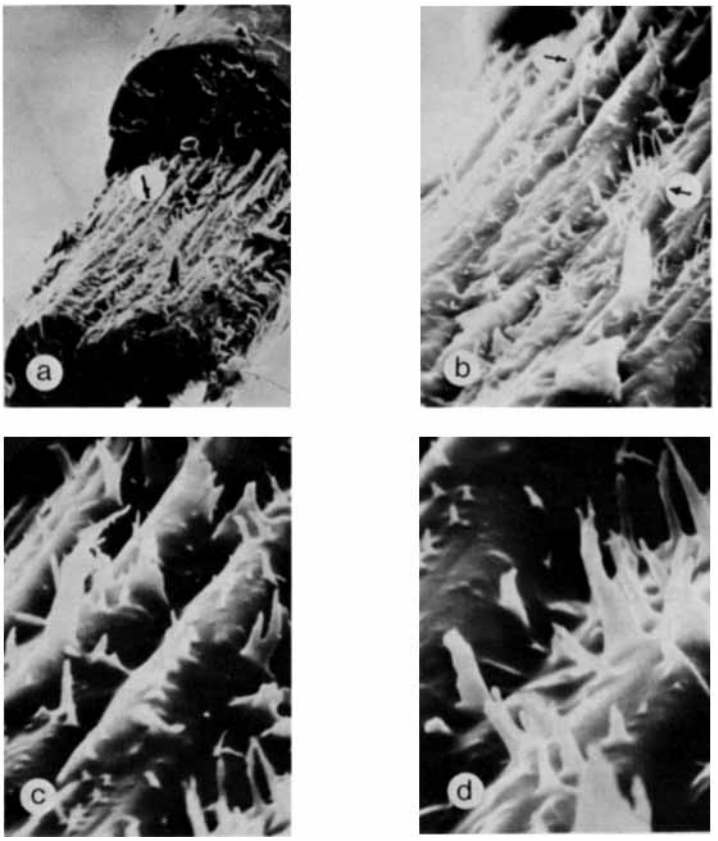

Fig. 24. Microscopic details of the split interface of an EDBH fiber fractured at 0% RH: (a) 1300 ×; (b) 2000 ×; (c) 5000 ×; (d) 7500 ×.

Sudden elastic recovery upon fracture sets up a shock wave which can rupture the fiber in weak areas. A strong, intact layer of cuticle cells is helpful in protecting the integrity of the fiber.

"Swelling" of the fracture tip and the onset of fibrillation are indicated in Figure 26. More severe fibrillation with destruction of the cortex is seen in Figure

Fig. 25. Axial split interface of an EDBH fiber fractured at 65% RH. Cortical cells seem to have been torn apart (6500 ×).

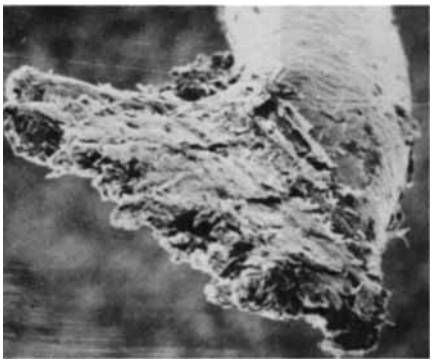

Fig. 26. Onset of fibrillation in a fracture end of EDBH fiber (450 ×).

27. Sometimes regions of the fiber removed from the fracture end are opened up, as shown in Figure 28, while the fracture end itself remains intact. The longitudinal cracks suggest that the transverse strength of the fiber in this region must have been low. Figure 29 shows a similar situation in the case of an abraded fiber. The splitting pattern suggests that longitudinal cracks developed during the abrading procedure may have brought about this type of damage.

This discussion indicates that the dissipation of elastic energy in the tensile fracture of a hair fiber might be a factor contributing to "split ends." It is easy to understand how combing long hair can result in tensile fracture leading to fibrillation if the comb hits an entanglement at the end of the hair assembly where the cuticle has been damaged through previous environmental or mechanical stresses.

Splitting tendency of sample J fibers: It has already been mentioned that fibers of samples J have "split end" problems. The difference between sample J and EDBH is especially striking at 65% RH where axial splitting in general is

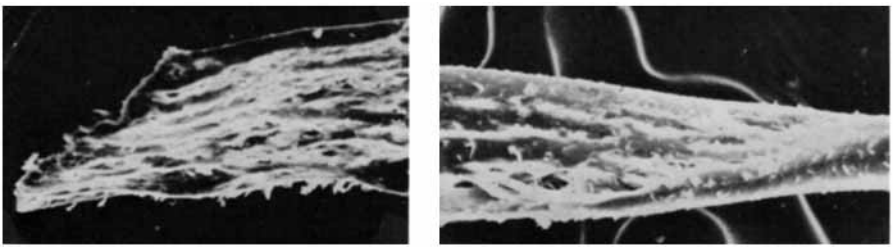

Fig. 27. Extensive fibrillation of a fracture end of a sample J fiber (225 ×).

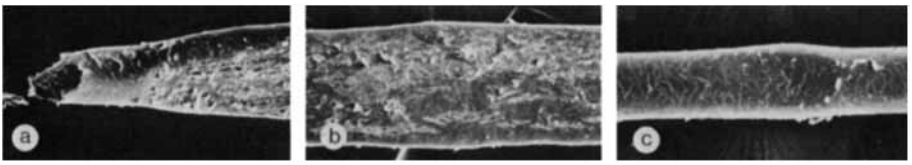

Fig. 28. Sample J fiber longitudinally shattered as a result of elastic dissipation (225 ×). Fracture end is intact in (a). An hump in (c) may be the same type of damage but limited by a strong cuticle.

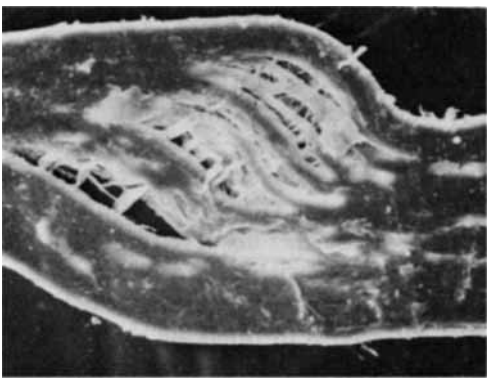

Fig. 29. Longitudinal fibrillation away from the fracture end. A abraded fiber from sample J (300 ×).

more probable (compare Figs. 3 and 4). It was of interest to determine whether structural differences between these fibers might be the cause of the greater splitting propensity of sample J. During the examination of fracture cross sections of fibers from the two sources, sample J fibers were generally found to have larger cross-sectional areas. A more detailed investigation was carried out by embedding 24 fibers each from EDBH and sample J in epoxy resin and examining cross-sectional cuts. The data in Table IV show little difference in the length of the minor axis but a significant difference in the length of the major axis and consequently in ellipticity and cross-sectional area. The cuticle thickness of the two fibers does not appear to be significantly different, although the low accuracy of this measurement with an optical microscope has to be taken into consideration. At high humidities the swelling of the cortex would be expected to exert higher pressure on the cuticle along the major axis, and hence the probability of fracture initiation in the vicinity of the major axis is increased.

Fracture faces of sample J fibers with smooth fractures (90% RH) were examined from this point of view. Of eight fibers with low cross-sectional area ($\sim 3.4 \times 10^{-9}$ m^2), equal numbers of fibers show fracture initiation in the vicinity of the major axis or the minor axis. However, of 10 fibers with high cross-sectional area ($\sim 5.2 \times 10^{-9}$ m^2), seven showed fracture initiation in the vicinity of the major axis and three in the vicinity of the minor axis. This lends support

TABLE IV
Geometrical Properties of EDBH and Sample J Fibers[a]

		EDBH	J
Major axis a (μm)		71 ± 3	93 ± 5
Minor axis b (μm)		62 ± 2	58 ± 2
Ellipticity a/b		1.17 ± 0.04	1.60 ± 0.11
Cross-sectional area (10^{-9} m^2)		3.46 ± 0.25	4.26 ± 0.28
Average cuticle thickness (μm)	Major axis	3.23 ± 0.15	2.81 ± 0.25
	Minor axis	3.18 ± 0.16	2.88 ± 0.20

[a] Each entry is an average of 24 specimens at the 95% confidence level.

to the fracture mechanism proposed in Figure 17. Fracture faces of wet fibers could not be used for this purpose, since many of them show fracture faces with no specific crack initiation [e.g., Fig. 15(b)]. It should be noted that these are rather tentative conclusions which must be confirmed with a larger specimen population.

Apart from fracture initiation, the size of the cross-sectional area of a fiber may be important from the point of view of axial splitting. In the case of nylon 66 monofilaments, Prevorsek et al.[14] observed that the breaking stress varied with increase in specimen volume with a sharp discontinuous decrease at a specific value, suggesting that flaw size may increase with the specimen volume. Although a significant difference in breaking stress is not observed between EDBH and sample J, the probability of finding a flaw on the surface of the medulla would be expected to increase with an increase in fiber cross section for the same specimen length. Since medullary structures can initiate or divert cracks, the splitting propensity of fibers of sample J may be due to the higher probability of encountering flaws as a result of larger cross-sectional area. Biogenetic factors may also play some role in this regard but are outside the scope of this investigation.

SUMMARY

Three types of fracture are encountered in the breaking of human hair subjected to longitudinal extension. These are (1) smooth fractures, (2) step fractures, and (3) fibrillated ends. Smooth fractures are generated by the propagation of a single crack perpendicular to the fiber axis. Step fractures seem to result from stress concentrations at the cracks which are relieved or diverted via the intercellular cement along the fiber axis, or by the simultaneous propagation of two cracks separated along the fiber axis and shearing along cortical cell surfaces. Fibrillated or split ends appear to be a result of postfracture dissipation of elastic energy.

Environmental humidity, i.e., the moisture content of the fiber, plays an important role in determining the nature of the fracture end. Greater numbers of smooth fractures are obtained at 0% and 90% RH and in wet fractures than at intermediate humidities (30% and 65% RH) where axial splitting occurs more frequently. Among other variables, a faster rate of extension seems to promote a larger number of smooth fractures. Surface deposition of polymers and surfactants appears to have little effect on the fracture behavior at treatment times ordinarily used in hair care.

Although the fracture behavior of hair is similar to that of nylon in some respects, the Griffith criterion of brittle fracture seems to be applicable to hair, whereas it does not hold for nylon monofilaments. After slow propagation of the primary crack, catastrophic failure of a hair fiber frequently seems to occur by secondary crack initiation near the periphery of the primary crack.

The greater tendency of fibers from a specific source to split may be due at least in part to larger fiber size, which increases the probability of flaws that can be effective in diverting cracks in the axial direction.

The intercellular cement seems to play an important role in stress transfer and axial splitting, and its influence requires further study.

The authors gratefully acknowledge the help of Ms. Hannelore Mark in performing the mechanical property measurements and thank Mr. John P. Hession for the electron microscope work reported

in this publication. Thanks are also due to Professor John C. Whitwell for his advice on the statistical interpretation of the data and to Dr. Harriet Heilweil for editing the manuscript and for useful suggestions regarding the content of the paper. The authors also thank Dr. G. E. R. Lamb for sharing his expertise on fiber fractography with them. These studies represent one aspect of work on the project "Studies on Modifications of Human Hair Properties by Surface Treatments," supported by a group of Corporate TRI Participants.

References

1. A. C. Brown and J. A. Swift, "Hair Breakage: The Scanning Electron Microscope as a Diagnostic Tool," *J. Soc. Cosmet. Chem.*, **26,** 289 (1975).

2. G. H. Henderson, G. M. Karg, and J. J. O'Neil, "Fractography of Human Hair," *J. Soc. Cosmet. Chem.*, **29,** 449 (1978).

3. J. W. S. Hearle, B. C. Jariwala, L. Konopasek, and B. Lomas, "Aspects of Fracture of Wool and Hair Fibers," *Proc. 5th Intl. Wool Text. Res. Conf. Aachen*, **II,** 370–379 (1975).

4. R. McGill, J. W. Tukey, and W. A. Larsen, "Variation of Box Plots," *Am. Statistician*, **32,** 12 (1978).

5. A. H. Bowker and G. J. Lieberman, *Engineering Statistics*, Prentice-Hall Inc., Englewood Cliffs, N.J., 1972, pp. 464–465.

6. R. E. Wilcox, W. L. Hightower, and R. V. Smith, "Post-hoc Data Analysis in Biomedical Research," *Am. Lab.*, **11,** 32 (1979).

7. B. C. Goswami and J. W. S. Hearle, "A Comparative Study of Nylon Fiber Fracture," *Text. Res. J.*, **46,** 55 (1976).

8. P. Alexander and R. F. Hudson, *Wool, Its Chemistry and Physics*, Frank Publishing Co., N.J., 1963, Figs. 1–14 opposite p. 5.

9. A. R. Bunsell, J. W. S. Hearle, L. Konopasek, and B. Lomas, "A Preliminary Study of the Fracture Morphology of Acrylic Fibers," *J. Appl. Polym. Sci.*, **18,** 2229–2242 (1974).

10. G. E. R. Lamb, "Studies of Tensile Failure in Oriented Polymer Fibers by Quantitative Fractography," *J. Polym. Sci., Polym. Phys. Ed.*, **20,** 297 (1982).

11. J. A. Kies, A. M. Sullivan, and G. R. Irwin, "Interpretation of Fracture Markings," *J. Appl. Phys.*, **21,** 716 (1950).

12. C. J. Monego and S. Backer, "Tensile Rupture of Blended Yarns," *Text. Res. J.*, **38,** 762–766 (1968).

13. C. E. Warburton, Jr., and J. C. Whitwell, "Multiple Points of Rupture in Textile Fibers, Part I: A Proposed Mechanism," *Text. Res. J.*, **36,** 887 (1966).

14. D. C. Prevorsek, A. B. Coe, and W. J. Lyons, "Behavior of Notched Fibers in Longitudinal Tension," *Text. Res. J.*, **35,** 878 (1965).

Received October 6, 1981
Accepted April 26, 1982